Motion of compactonlike kinks

P. Tchofo Dinda, T. C. Kofane,* and M. Remoissenet
Laboratoire de Physique, Université de Bourgogne, 9 Avenue Alain Savary, Boîk Postale 47870, 21078 Dijon, France
(Received 5 August 1999)

We analyze the ability of a compactonlike kink (i.e., kink with compact support) to execute a stable ballistic propagation in a discrete Klein-Gordon system with anharmonic coupling. We demonstrate that the effects of lattice discreteness, and the presence of a linear coupling between lattice sites, are detrimental to a stable ballistic propagation of the compacton, because of the particular structure of the small-oscillation frequency spectrum of the compacton in which the lower-frequency internal modes enter in direct resonance with phonon modes. Our study reveals the parameter regions for obtaining a stable ballistic propagation of a compactonlike kink. Finally we investigate the interactions between compactonlike kinks. [S1063-651X(99)14412-X]

PACS number(s): 41.20.Jb, 46.40.−f, 02.30.Jr

I. INTRODUCTION

Many nonlinear lattice models give rise to energy localization effects—and hence support stable kink structures such as the sine-Gordon [1,2], the double sine-Gordon [3], or the Φ-four [4] lattices. These lattice models consist of harmonically coupled particles submitted to an on-site substrate potential which possesses several degenerate minima. This spatial degeneracy, associated with the linear coupling between lattice sites, leads to a kink structure with infinite wings, which causes mutual interactions between adjacent kinks. On the other hand, Rosenau and Hyman [5], who investigated a special type of Korteweg–de Vries equations, discovered that solitary waves may compactify in the presence of a nonlinear dispersion. Such solitary waves, which are characterized by a compact support, i.e., the absence of infinite tail, have been called *compactons*. Subsequently, Kivshar [6] reported that intrinsic localized modes in purely anharmonic lattices may exhibit compactonlike properties. Recently, Dusuel *et al.* [7] demonstrated that the same phenomenology can also appear in nonlinear Klein-Gordon systems with anharmonic coupling, then obtained the experimental evidence of the existence of a static compacton in a real physical system, made up by identical pendulums connected by springs. Very recently, dark compacton solutions have been found in a model of Frenkel excitons [8]. In general, one of the lines of current research focuses on the operating conditions for generating compactonlike structures in real physical systems in which the compacton's properties could ensure practical applications. In this context, an understanding of the dynamical properties of those compactons is essential in gaining some insight into the operating conditions in which real physical systems can support such compact structures. In fact, since the pioneering work of Rosenau and Hyman [5,9], there are many problems which are challenging and interesting, which have not been sufficiently understood theoretically. In this respect, a fundamental question arises [7] as to whether a compactonlike kink (CK) is able to execute a stable ballistic propagation in nonlinear Klein-Gordon systems. Indeed, Dusuel *et al.* [7] reported that a CK, when moving in the continuum lattice, executes a phonon radiation process which ends up by damping its motion. Now, it is well known that the phonon radiation produced by classical kink structures is quite negligible in a continuum lattice, as well as the radiative reaction on the kink's dynamics.

In this paper we resolve this contradiction by treating intrinsically the lattice discreteness without approximation, and we show that most of the dynamical properties of a CK are atypical and do not fit into the general picture that describes behavior found in classical field theories. In particular we elucidate the dynamical mechanism which gives rise to the spontaneous emission of phonon radiation from a continuum CK, and point out the radiative reaction on the CK dynamics. Our study reveals the parameter regions for obtaining a stable ballistic propagation, and the essential features of the interaction between compactons.

In the following section we define the Φ-four model under consideration and in Sec. II B we examine the frequency spectrum of the system. Section III is devoted to an examination of discreteness effects on a CK. In Sec. IV we perform the molecular dynamics simulation of the ballistic propagation of a CK, and examine the interaction between compactons. We conclude in Sec. V.

II. STATIC AND DYNAMICS PROPERTIES

A. The model

The system under consideration is a Φ-four lattice with linear and nonlinear coupling between lattice sites, governed by the following Hamiltonian:

$$H=\sum_n \frac{1}{2}\dot{Q}_n^2+\frac{1}{2}C_l(Q_n-Q_{n-1})^2+\frac{1}{4}C_{\mathrm{nl}}(Q_n-Q_{n-1})^4 + \frac{1}{8}\omega_0^2 V(Q_n), \tag{1}$$

where Q_n is the position of the nth particle measured from the nth lattice site, C_l and C_{nl} are parameters that control the strength of the linear and nonlinear coupling, the dot indicates the time derivative, ω_0 is the limiting frequency for

*Permanent address: Université de Yaoundé I, Departement de Physique, BP 812, Yaoundé, Cameroon.

long wavelength excitations. In the present work, we take $\omega_0=2\sqrt{2}$, to facilitate the comparison of our results with previous work [7]. In Eq. (1), $V(Q_n)\equiv(1-Q_n^2)^2$ is the on-site potential. The *potential energy* of the system is defined by

$$E_p=\sum_n \frac{1}{2}C_l(Q_n-Q_{n-1})^2+\frac{1}{4}C_{\rm nl}(Q_n-Q_{n-1})^4 + \frac{1}{8}\omega_0^2 V(Q_n). \tag{2}$$

The equation of motion for the system is

$$\ddot{Q}_n=C_l(Q_{n+1}+Q_{n-1}-2Q_n)+C_{\rm nl}[(Q_{n+1}-Q_n)^3 + (Q_{n-1}-Q_n)^3]+\frac{1}{2}\omega_0^2(Q_n-Q_n^3). \tag{3}$$

Note that for $\omega_0^2 \ll C_l$, or $\omega_0^2 \ll C_{\rm nl}$, one approaches the continuum limit, in which Q_n varies slowly from one site to another. Using the continuum limit approximations, Eq. (3) can be reduced to a partial differential equation that admits, for $C_{\rm nl}=0$, the well-known Φ-four kink solution [10]

$$\phi(x)=\tanh[\beta_K(x-X)], \quad \beta_K\equiv[\omega_0^2/(4C_l)]^{1/2}, \tag{4}$$

whereas for $C_l=0$, one obtains the following compactonlike kink solution (kink with compact support) [7]:

$$\begin{cases} f(x)=\pm\sin[\beta_C(x-X)] & \text{for } |x-X|\leqslant\xi=\pi/(2\beta_C), \\ f(x)=\pm 1 & \text{for } |x-X|>\xi, \quad \beta_C\equiv[\omega_0^2/(6C_{\rm nl})]^{1/4}. \end{cases} \tag{5}$$

In Eqs. (4),(5), the site index n is replaced by the continuous position variable x (the lattice spacing being assumed to be equal to 1), X locates the c.m. (center of mass) of the system. Whereas a standard kink possesses exponential (infinite) wings [see Eq. (4)], the full width of the CK is strictly limited to [see Eq. (5)]

$$L_C=\pi/\beta_C=\pi[6C_{\rm nl}/\omega_0^2]^{1/4}. \tag{6}$$

This implies that, in principle, a compacton and an anticompacton will not interact unless they come into contact in a way similar to the contact between two hard spheres. Figure 1(a) shows plots of the exact profile Q_n of the static CK (solid curve) for $L_C=50$ and $L_C=500$. Note that the discrete solution Q_n is obtained through a relaxation process [1,2]. We accomplish the relaxation by, first, putting the continuum CK in the discrete lattice so that the center of the CK is located on a particle near the middle of the chain. Then, using molecular dynamics, one extracts energy from the system to relax the chain by periodically setting the velocities of all the particles to zero after a specified number of time steps. The dotted curves in Fig. 1(a) show the profiles of the discrete Φ-four kinks having the same slope as those of the CK's under consideration ($\beta_C=\beta_K$). One can clearly identify in Fig. 1(a) the exponential wings of the kink, in comparison with the strictly limited wings of the CK. Furthermore, one can easily measure the correctness of the analytical continuum solution (5) by evaluating the static

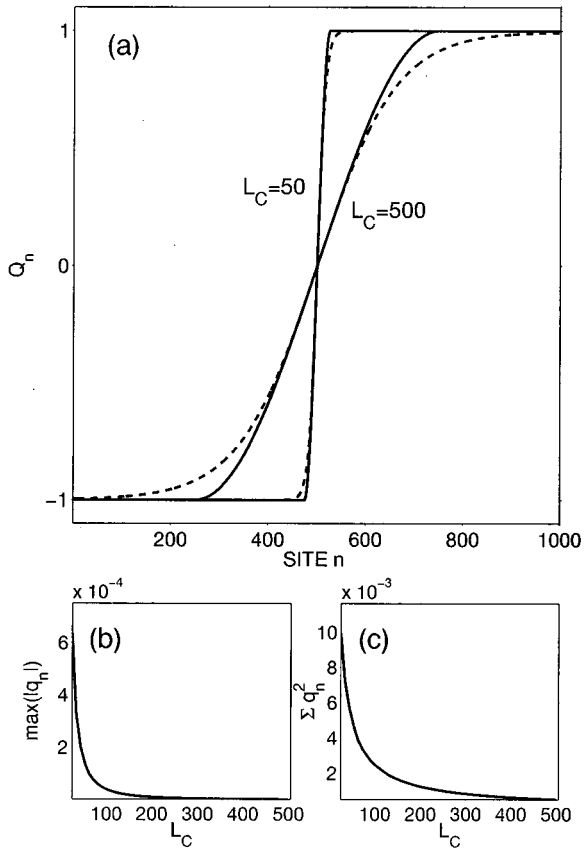

FIG. 1. (a) Plot showing the static profile of the compactonlike kink ($C_l=0$) for $L_C=50$ and $L_C=500$ in a discrete lattice of 1000 particles. The CK is located at $X=500$. The solid curve represents the exact discrete CK solution ($C_l=0$). The dashed curve represents the discrete Φ-four kinks ($C_{\rm nl}=0$) having the same slope ($\beta_C=\beta_K$) as of those of the compactons under consideration. (b) Maximum value of the static dressing $\gamma=\max(|q_n|)$ as a function of the compacton width L_C. (c) Value of the deviation $\xi=\Sigma q_n^2$ as a function of L_C.

dressing of the continuum CK, $q_n=Q_n-f_n$, where f_n is the continuum solution evaluated at discrete lattice points. Two measures of the correctness of f_n are the maximum value of the static dressing $\gamma=\max(|q_n|)$, and the deviation $\xi=\Sigma q_n^2$. Figures 1(b)–1(c) show the results obtained for $25\leqslant L_C \leqslant 510$. For example, for $L_C=50$, γ and ξ do not exceed 1.6×10^{-4} and 5×10^{-3}, respectively. Moreover, both γ and ξ decrease monotonically to zero as L_C increases. This decrease implies that the solution f_n provides a highly accurate representation of the discrete CK solution Q_n for a sufficiently large CK (or equivalently, for a sufficiently large nonlinear coupling $C_{\rm nl}$), and coincide exactly with Q_n in the continuum limit.

On the other hand, Dusuel *et al.* [7] reported that a CK can execute a stable ballistic propagation in a continuum lattice, but with a single velocity $V=\sqrt{C_l}$, implying that the presence of harmonic coupling forces between the lattice sites ($C_l\neq0$) is required for a CK to propagate. We will show below that, contrary to this continuum theory [7], the discretized field theory predicts the existence of a translation mode for a CK, at any nonrelativistic velocity. In fact, most of the dynamical properties of a CK are readily understood

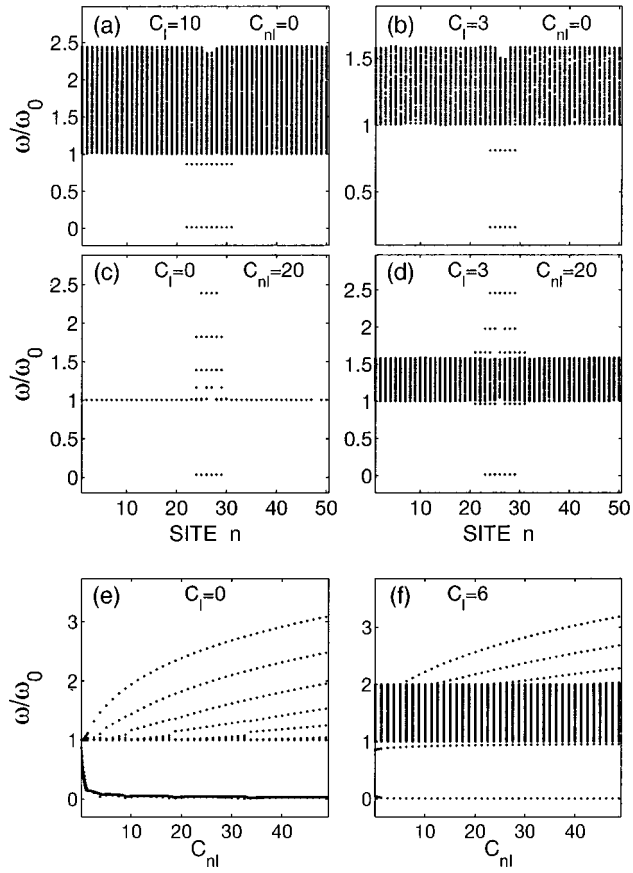

FIG. 2. (a)–(d) show the temporal Fourier transform of the small amplitude motion of a compactonlike kink in a 50 particle chain. (e) and (f) show the spectra obtained from the linear operator $\mathcal{L}$, Eq. (12). The solid curve in (e) corresponds to the c.m. mode ω_X/ω, Eq. (10).

by looking into the structure of the small-oscillation frequency spectrum of the system.

B. Frequency spectrum of the system

Some fundamental features of classical kink's dynamics are recalled in Figs. 2(a) and 2(b), that we obtained by performing a Fourier transform of Eq. (3) (with $C_{\rm nl}=0$), in which the initial condition of the dynamics was the discrete static solution Q_n and a weak noise on each particle of the lattice. As Figs. 2(a), 2(b) show, the frequency spectrum of a kink consists of a phonon band $\omega=\omega_0[1+(4C_l/\omega_0^2)\sin^2(k/2)]^{1/2}$, $0\leqslant k\leqslant\pi$, which depends on C_l and exists whether the kink is present or not in the lattice. When the kink is present in the lattice, one or several additional frequencies known as collective modes appear in the spectrum, below the lower-phonon band edge $\omega<\omega_0$. A well known example of collective mode is the c.m. mode. In the continuum system, the c.m. mode is the zero-frequency Goldstone mode $\omega_X=0$ [see Fig. 2(a)], which corresponds to a particlelike translation of the kink. In the discrete system, the c.m. mode becomes a finite-frequency mode associated with oscillations of the kink in the Peierls-Nabarro (PN) potential [see Fig. 2(b)]; this frequency is known as the PN frequency. Now, Fig. 2(c), which shows the spectrum that we obtained for $C_l=0$, reveals one of the main results of the present research, that is, the fact that *a* CK *possesses a zero-frequency Goldstone mode for sufficiently large* $C_{\rm nl}$, *which indicates that in the limit of no perturbations a CK can execute a stable ballistic motion at any nonrelativistic velocity.* We attribute the failure of the continuum field theory [7] for predicting this translation mode of a CK to the fact that some self-consistency conditions of the continuum limit approximations (CLA's) are not fully satisfied by the continuum solution $f(x)$ given by Eq. (5). Indeed in standard CLA's one expands the discrete finite differences $Q_{n\pm1}-Q_n$ in Taylor series and keeps only the leading terms (for obtaining the continuum solution of the equation of motion), by assuming that the higher-order terms of the expansion are negligible. The continuum solution hence obtained $f(x)$ must therefore be self-consistent with the assumption just mentioned. Now, the higher-order derivatives of $f(x)$, Eq. (5), contain the Dirac δ function or its derivatives $\delta',\delta'',\ldots$, at the edges of the CK, which yield non-negligible contributions for terms which have been neglected in the CLA's, hence the failure of the continuum field theory. Nevertheless, the solution $f(x)$ provides the exact representation of the shape of a static CK.

In addition to the c.m. mode, the kink can execute internal vibrations that are commonly referred to as the internal modes. The most common internal mode that kinks possess is that corresponding to an oscillation of the kink width about an equilibrium value. This internal mode is known as the *shape* mode of the kink. In Figs. 2(a) and 2(b) one clearly identifies the shape mode of the Φ-four kink, just below the lower phonon band edge. Although the Φ-four kink possesses only one internal mode, the number of internal modes in classical kink-bearing systems may increase without bound as a function of the anharmonicity of the substrate potential [11], but the fundamental feature of these internal modes is that they always appear in the gap below the lower-phonon band edge: $\omega<\omega_0$. Quite in contrast, we observe in Fig. 2(c) the surprising result that the nonlinear coupling $C_{\rm nl}$ induces, within a CK, a large number of internal modes that are all located above the characteristic frequency ω_0: $\omega>\omega_0$. Furthermore, Fig. 2(d) shows that the linear coupling induces two fundamental features in the spectrum: first, an internal mode just below ω_0, and second, a phonon band above ω_0, whose size increases as C_l increases. Consequently, if the phonon band is sufficiently large, some internal modes of the CK will appear in the phonon band and make direct resonance with phonons, thus producing a continuous stream of phonons. Such a radiative process differs drastically from the behavior found in classical kink-bearing systems, in which the fundamental frequency of the kink's motion always like outside the phonon band, and there, the phonon-radiation mechanism results from the resonance of the harmonics of this frequency with the phonon modes [1–3,10]. Furthermore, it should also be emphasized that the number of internal modes of a CK increases without bound as $C_{\rm nl}$ increases [see Fig. 2(e)], thereby increasing the number of internal modes that fall in the phonon band when $C_l\neq0$ [see Fig. 2(f)]. Thus, the mechanism of direct resonance with phonons, which causes radiation of energy away from a CK even for small-amplitude dynamics, alters unavoidably the fundamental properties of the CK (e.g., its compact support). Furthermore, a CK is subject to other effects, such as

discreteness effects, that may alter its dynamical properties, as we discuss below.

III. DISCRETENESS EFFECTS IN A CK BEARING SYSTEM

A simple way to analyze the effects of lattice discreteness on the dynamics of a CK is an examination of the frequency of the c.m. mode, whose value generally serves as a measure of whether a system will exhibit *discrete* or *continuum* behavior. To this end, we use a collective variable theory in order to calculate a lowest-order expression for the frequency with which a CK executes a trapped oscillatory motion of small amplitude in the PN well, that is, we decompose the field Q_n in the following way:

$$Q_n = f_n + q_n, \quad \begin{cases} f_n(X) = \pm \sin[\alpha(n-X)] & \text{for } |n-X| \leqslant \xi \\ f_n(X) = \pm 1 & \text{for } |n-X| > \xi, \end{cases} \tag{7}$$

where f_n is the continuum CK solution, Eq. (5), evaluated at discrete lattice points. Note that one must add the term q_n in Eq. (7) in order to account for the dressing of the continuum CK. Notice also that we consider here the case where $C_l = 0$, in which the ansatz function f_n provides a best representation of the CK profile. Then, using a projection-operator approach [12], that is, substituting the ansatz Eq. (7) into the discrete equation of motion (3) and projecting the resulting equation in the direction $\langle f_{n,X}|$ yields the following equation of motion for the collective variable X:

$$\ddot{X} = \frac{1}{M - \langle f_{n,XX}|q_n\rangle}\left[\dot{X}^2(\langle f_{n,XXX}|q_n\rangle - \langle f_{n,X}|f_{n,XX}\rangle) + 2\dot{X}\langle f_{n,XX}|\dot{q}_n\rangle + C_{\rm nl}\langle f_{n,X}|\Delta_4(f_n+q_n)\rangle - \frac{\omega_0^2}{8}\langle f_{n,X}|V'(f_n+q_n)\rangle\right],$$

$$\Delta_4 h_n \equiv (h_{n+1}-h_n)^3 + (h_{n-1}-h_n)^3, \tag{8}$$

where X after a comma stands for partial differentiation with respect to X, the bracket notation means sum over the particle index, and $M \equiv \langle f_{n,X}|f_{n,X}\rangle$ is the compacton mass. Then setting $q_n = 0$ for all n (the approximation of setting $q_n = 0$ is called the ''bare approximation''), and neglecting the small terms of order $\dot{X}^2$, Eq. (8) becomes

$$\ddot{X} = \frac{1}{M}\left[C_{\rm nl}\langle f_{n,X}|\Delta_4(f_n)\rangle - \frac{\omega_0^2}{8}\langle f_{n,X}|V'(f_n)\rangle\right]. \tag{9}$$

By decomposing X as $\mathrm{int}(X)+R$, where $\mathrm{int}(X)$ represents the integral part of X, then setting $R=\eta$ or $R=\frac{1}{2}+\eta$ (depending on whether the stable equilibrium position of the c.m. is located on a lattice site or midway between two adjacent sites) and linearizing in η, Eq. (9) becomes $\ddot{\eta} = -\omega_X^2\eta$, where

$$\omega_X^2 = \frac{\alpha}{M}\Bigg[C_{\rm nl}\Bigg\{\frac{1}{4}H_1(2\alpha) - \frac{1}{2}H_1(\alpha) + \left(-\frac{3}{2} + 3\cos\alpha - \cos^3\alpha\right)H_2(\alpha) + \left(-\frac{3}{4} + \frac{3}{2}\cos^2\alpha - \cos^3\alpha\right)H_2(2\alpha) + \left(-\frac{9}{4} + \frac{3}{2}\cos\alpha - \frac{1}{2}\cos^3\alpha\right)D_1(\alpha) + \left(-\frac{3}{8} + \frac{3}{4}\cos^2\alpha - \frac{1}{2}\cos^3\alpha\right)D_1(2\alpha) - \frac{7}{4}D_2(\alpha/2) + \frac{\sin^3\alpha}{2}D_2(\alpha) + \frac{3}{4}D_2(3\alpha/2) + \left(\frac{3}{8}\sin(2\alpha) - \frac{3}{4}\sin\alpha + \frac{1}{2}\sin^3\alpha\right)D_2(2\alpha)\Bigg\} + \frac{\omega_0^2}{8}\left\{H_1(\alpha) + \frac{1}{2}H_1(2\alpha)\right\}\Bigg], \tag{10a}$$

$$H_1(z) \equiv \frac{-2z\sin(zN)}{\sin(z)}, \quad H_2(z) \equiv \frac{-2z\sin[z(N-2)]}{\sin(z)},$$

$$D_1(z) \equiv -4z\cos[z(N-1)],$$

$$D_2(z) \equiv -4z\sin[z(N-1)], \quad M = \frac{\alpha^2}{2}\left[N + \frac{\sin(\alpha N)}{\sin(\alpha)}\right],$$

$$N = \mathrm{int}(\xi+R) + \mathrm{int}(\xi-R) + 1. \tag{10b}$$

We can check the accuracy of our lowest-order expression for ω_X, Eq. (10), by performing numerically the exact determination of the small-oscillation spectrum of the system in the presence of a stable CK ψ_n (that we obtained via a classical pseudodynamics relaxation process). That is, we consider $Q_n(t) = \psi_n(X_{eq}) + \epsilon\lambda_n(X_{eq})\exp(-i\omega t)$, where ϵ is a small parameter. The linearization of the discrete equation of motion, Eq. (3), about ψ_n yields the following eigenvalue equation:

$$\mathcal{L}[\lambda_n] = \omega^2[\lambda_n], \tag{11}$$

where $[\lambda_n]$ is an eigenvector, the nonzero components of the linear matrix operator $\mathcal{L}$ are

$$\mathcal{L}(i,i\pm1) = -C_l - 3C_{\rm nl}(\psi_{i\pm1} - \psi_i)^2, \tag{12a}$$

$$\mathcal{L}(i,i) = 2C_l + 3C_{\rm nl}[(\psi_{i+1}-\psi_i)^2 + (\psi_{i-1}-\psi_i)^2] - \frac{\omega_0^2}{2}(1-3\psi_i^2), \tag{12b}$$

$$\mathcal{L}(1,1) = C_l + 3C_{\rm nl}(\psi_2-\psi_1)^2 - \frac{\omega_0^2}{2}(1-3\psi_1^2),$$

$$\mathcal{L}(1,2) = -C_l - 3C_{\rm nl}(\psi_2-\psi_1)^2, \tag{12c}$$

$$\mathcal{L}(N,N-1) = -C_l - 3C_{\rm nl}(\psi_{N-1}-\psi_N)^2,$$

$$\mathcal{L}(N,N)=C_l+3C_{\rm nl}(\psi_{N-1}-\psi_N)^2-\frac{\omega_0^2}{2}(1-3\psi_N^2). \tag{12d}$$

Figure 2(e) shows the variations of ω_X (solid curve) together with the exact determination of the c.m. frequency $\omega_{X\ \rm exact}$ obtained via the linear operator $\mathcal{L}$ (dotted curve). We observe that for small $C_{\rm nl}$, the system exhibits a *discrete* behavior, in which the c.m. frequency is not zero, and decreases strongly as $C_{\rm nl}$ increases. When $C_{\rm nl}$ is sufficiently large, the c.m. mode becomes the zero-frequency Goldstone mode. Furthermore, quantitatively, the value of ω_X agrees more or less well with $\omega_{X\ \rm exact}$ depending on the value of $C_{\rm nl}$. But the general qualitative agreement is excellent. Thus, the above results show that discreteness effects become significant for $C_{\rm nl}<10$. These effects can therefore be avoided by using a sufficiently large nonlinear coupling, for obtaining the untrapped regime of a CK, that we consider below.

IV. BALLISTIC PROPAGATION AND INTERACTIONS BETWEEN COMPACTONS

A. Ballistic propagation

As discussed in the preceding section, one of the main results of the present work is the demonstration that a CK possesses a zero-frequency Goldstone mode for sufficiently large $C_{\rm nl}$ [see Fig. 2(c)]; which indicates that a CK can execute a stable ballistic motion at any nonrelativistic velocity. To observe this propagation regime, we have performed numerical simulations of Eq. (3), for $C_{\rm nl}=14500$, $C_l=208$, and $C_l=0$, respectively. Our simulations start with a CK located at the middle of a 3000 particle chain, with initial velocity $V_0\equiv\dot{X}(t=0)>0$, which induces the following particle velocities: $\dot{Q}_n=V_0 f_{n,X}+\dot{q}_n(0)$, that we have approximated by $\dot{Q}_n=V_0 f_{n,X}$, as we do not have the $\dot{q}_n(0)$'s. Although this approximation is valid when discreteness effects are negligible, such an initial condition acts as a source of perturbations which excites the whole frequency spectrum. Figures 3 show the lattice profile after the CK has traveled over 1100 lattice spacings. As can be seen in Fig. 3(a), when $C_l=208$, a strong phonon radiation occurs in the backward direction of the moving CK, due to direct resonance of the internal modes of the compacton with phonon modes, as we mentioned above. This radiative process alters the compact support of the CK and causes a small decrease of its velocity. When $C_l=0$ the phonons are created at frequency ω_0, but these phonons cannot propagate owing to their zero group velocity [see Fig. 3(b)]. For large V_0 and $C_l=0$, the effects of the initial perturbations are significantly enhanced, which causes a continual decrease of the velocity $\dot{X}(t)$. But we see in Figs. 3(c), 3(d), 3(e), and 3(f) that for a small velocity V_0, the perturbations induced by the launching conditions are significantly reduced, as well as the resulting radiative process. Nevertheless, the Poynting flux evaluated at the site $n=1000$ shows that although the radiation is small it is not zero for $C_l\neq 0$ [see Fig. 3(e)]. Note that the discrete definition of the Poynting flux S is [2]

$$S(n,t)=[Q_{n+1}(t)-Q_n(t)]\frac{Q_n(t+\Delta t)-Q_n(t)}{\Delta t}. \tag{13}$$

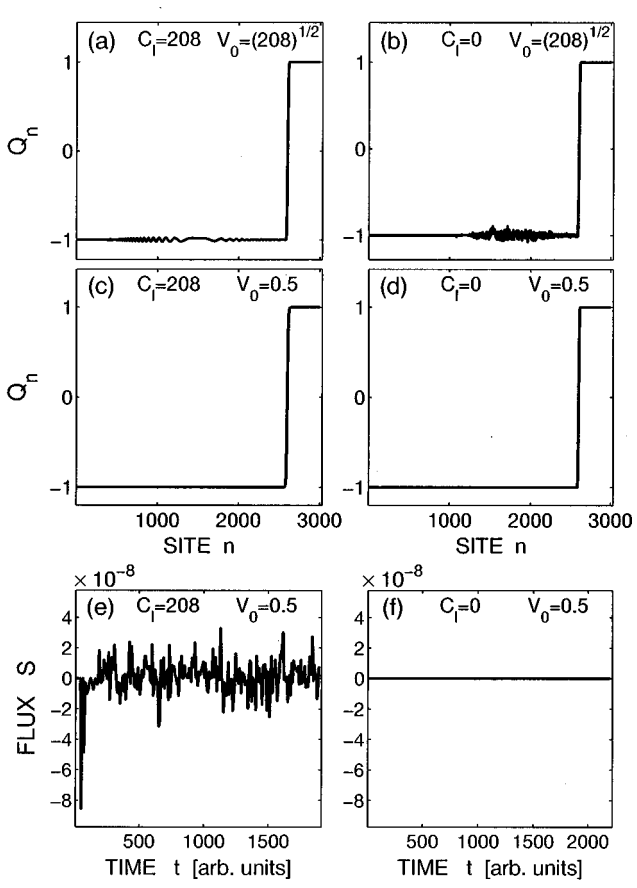

FIG. 3. (a)–(d) show the profile of compactonlike kink after traveling on 1100 lattice sites, for $C_{nl}=14500$. The dashed curves show the initial kink profile. Simulation parameters are (a) $C_l=208$, $X(t=0)=1500$, $V_0=\dot{X}(t=0)=\sqrt{208}$. (b) $C_l=0$, $X(t=0)=1500.5$, $V_0=\sqrt{208}$. (c) $C_l=208$, $X(t=0)=1500$, $V_0=0.5$. (d) $C_l=0$, $X(t=0)=1500.5$, $V_0=0.5$. (e) and (f) show the instantaneous Poynting flux evaluated at site $n=1000$, during the dynamics in (c) and (d), respectively.

For $C_l=0$, the whole phonon packet reduces to standing waves at frequency ω_0. Consequently the sites located far away from the CK are not perturbed by the CK motion when $C_l=0$ [see Fig. 3(f)].

B. Interactions between compactonlike kinks

The problem of interactions between CK's was briefly examined by Dusuel *et al.* [7], who reported that the head-on collision between compactons traveling at a specific velocity is inelastic, leading to kinks after the collision. This result means that the two colliding CK's can survive a collision through a conversion into standard kink structures [7]. In fact, by carefully analyzing the collision process, we show below that CK's do not survive a head-on collision whatever are their incoming velocities, in contrast to standard kinks which are known to survive collisions in some ranges of incoming velocities. In this context, it is worth recalling that the interaction between standard kinks have been intensively investigated [13–17]. It was reported in most of these studies that there exist some ranges of initial kink velocities for which the collisions end in reflection, and that these reflec-

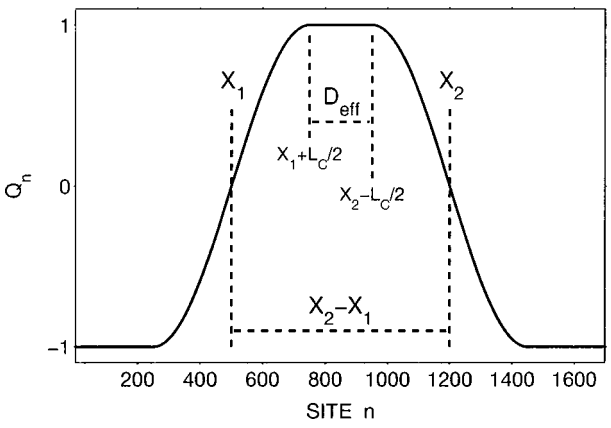

FIG. 4. Plot illustrating the initial profile of the lattice with a static compacton ($L_C=500$) and an anticompacton ($L_C=500$) before the beginning of the collision process.

tion regions alternate with regions of incoming velocities for which the collisions end in a bound pair of kink-antikink. Moreover, an outstanding result of these studies is the demonstration that the excitation of the internal mode of the kink during the collision (when this mode exists) gives rise to physical phenomena which determine the type of entities which emerge from the collision process. For example, Campbell *et al.* [13], who studied kink-antikink collisions in classical kink-bearing systems, observed from simulations that there exist some particular ranges of incoming velocities for which the colliding kinks form a temporary bound pair after the initial collision. During this first collision, some energy of translation from each kink is transferred to their internal modes, the translation energy thereby being reduced sufficiently such that the colliding kinks form a temporary bound state. While in this bound state, they collide a second time, permitting a sufficient amount of energy which has been transferred to the internal modes to be transferred back to the translation mode of each kink, thus allowing them to become again an unbound pair and separate to infinity. Therefore, the question arises as to whether or not the above mentioned phenomena may occur in CK-bearing systems. To answer this question we have carried out numerical simulations of collisions between compactons, which will be presented below, by taking an extreme care of the sensitivity of the compacton dynamics to the approximate nature of the initial velocities of the particles (as we already mentioned in the previous section). In this respect, it is useful to carefully monitor a characteristic parameter which can serve as a measure of the quality of launching conditions. A simple parameter (criterion) that can be used is the interaction energy of a pair of CK's. The interaction energy of two colliding entities at a given time $tE_{\rm int}$, may be defined as the potential energy of the system time t, measured from the potential energy of a system of two noninteracting compactons E_{p0}:

$$E_{\rm int} \equiv |E_p - E_{p0}|/E_{p0}. \tag{14}$$

Thus, if the launching conditions are perfectly controlled, then this interaction energy will remain strictly at zero until the two CK's come into contact. On the other hand, as illustrated in Fig. 4, it is important to make here a clear distinc-

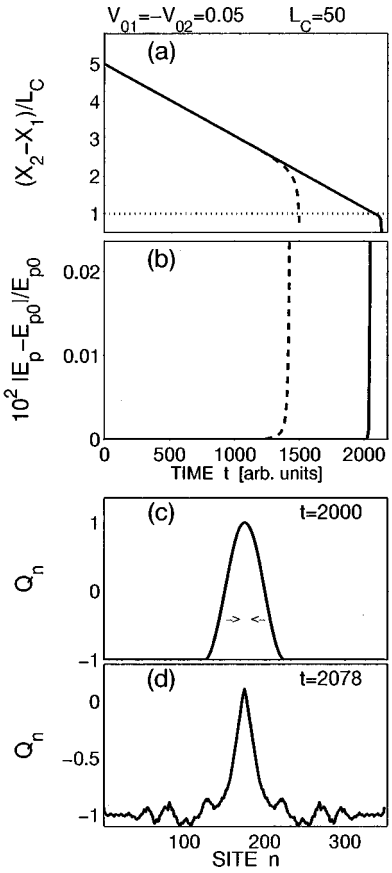

FIG. 5. Plot showing the collision process of a compacton traveling at velocity $V_{01}=0.05$ ($L_C=50$) and an anticompacton traveling at velocity $V_{02}=-V_{01}$ ($L_C=50$). (a) Time evolution of the normalized separation distance between the center-of-masses of the two compactons. (b) Time evolution of the interaction energy. (c) System profile at time $t=2000$. (d) System profile at time $t=2078$.

tion between the distance between the center-of-masses of the two CK's, X_2-X_1, and the effective separation distance which is

$$D_{\rm eff}=(X_2-L_C/2)-(X_1+L_C/2)=X_2-X_1-L_C. \tag{15}$$

In principle, if $X_2-X_1>L_C$, then two compactons will not interact. They will begin to interact as soon as X_2-X_1 will become less or equal to L_C (i.e., as soon as $D_{\rm eff}\leqslant 0$). In all our simulations of collisions between CK's, the initial positions of the c.m.'s, $X_1(t=0)$ and $X_2(t=0)$, were chosen such that $D_{\rm eff}(0)=200$, to facilitate the comparison between different cases. Figures 5(a), 5(b), 5(c), and 5(d) show the collision process of a CK [with $L_C=50$, $X_1(t=0)=50$, in a 349 particle lattice, and initial velocity $V_{01}=0.05$] and anti-CK [with $L_C=50$, $X_2(t=0)=300$, and initial velocity $V_{02}=-0.05$], represented in solid curves. As Fig. 5(a) shows, as soon as the two compactons are launched, the separation distance between their c.m.'s continually decreases without inducing a change in the interaction energy [see Fig. 5(b)], which remains to zero until the time $t=2000$. At this time, we observe in Fig. 5(a) that $X_2-X_1=L_C$, thus indicating that the two compactons come into contact in a way similar to the contact between two hard spheres [see Fig. 5(c)]. Here lies a fundamental difference

between compactons and standard kinks. The dotted curves in Figs. 5(a) and 5(b), which illustrate the interaction of a pair of Φ-four kinks having the same slope and same initial velocities as those of the compactons, demonstrate that the interaction between Φ-four kinks begins much earlier ($t \approx 1436$) than in the case of compactons ($t=2000$). Note that the value of C_l for which the Φ-four kink and the CK have the same slope ($\beta_K=\beta_C$) is given by

$$C_l=\frac{\omega_0}{4}\sqrt{6C_{\rm nl}}. \tag{16}$$

This Φ-four collision process ends in a bound state not represented in Figs. 5. On the other hand, the collision between CK's also ends in an unstable bound state, in which the newly formed entity executes an unstable breathing motion, which progressively destroys the compact support of the energy localization [see Fig. 5(d)].

To check the behavior of CK's during collisions, we have carried out, in a systematic manner, numerical simulations in a wide range of initial velocities including low and high velocities. It comes out from those simulations that *collisions between the compactons that travel at low incoming velocities always end in a bound state* [such as in Figs. 5]. The main results for high incoming velocities are summarized in Fig. 6. Figures 6(a1), 6(b1), 6(c1), and 6(d1), which show the collision process of two compactons with initial velocities ±10 and the same width $L_C=50$, would indicate that the collision ends in reflection. This type of collision corresponds to the situation that was considered in Ref. [7] and was referred to as an inelastic collision. In fact, a careful examination of the system's profile at the very beginning of the collision reveals quite clearly that the two colliding entities are not compactons in the strict sense [see Fig. 6(c1)]. Indeed, a small but non-negligible part of the energy that was initially strictly localized within the compactons ultimately finds itself away from the support of the two compactons, in the form of strong noise. The presence of this noise is due to the difficulty of perfectly controlling the launching conditions of the compactons, as a result of the approximation of neglecting the effects of the static dressing [$\dot{q}_n(0)=0$] in the initial velocities on the particles. Consequently, as one starts with highly accurate initial conditions but which are not the exact solution for the system, the initial conditions behave as a source of noise which is subsequently amplified in time. However, as we already mentioned in Sec. IV A, the effects of the static dressing can be minimized by just minimizing the discreteness effects, or equivalently, by increasing the width of the compacton. Figures 6(a2), 6(b2), 6(c2), and 6(d2), which show the collision process of two compactons which are launched with the same initial velocities as in Figs. 6(a1), 6(b1), 6(c1), and 6(d1) but with a much larger width, $L_C=500$, reveal that the collision between compactons with incoming velocities ±10 ends in fact in an unstable bound state. In general, we have found out the fundamental result that *collisions between compactons never end in reflection* for any incoming velocities, including the cases where two compactons are launched with different velocities, and the case of collisions of compactons with different widths. Thus, all the translation energy of compactons is transferred to their internal modes during the collision. To explain this behavior, one must be aware of the fact that the reflection back of two colliding entities requires that most of the energy lost by the c.m. mode in the beginning of the collision is subsequently restored. In the Φ-four kink system, in which only a single internal mode exists, a direct energy exchange process occurs between the c.m. mode and the internal mode, thus allowing reflection back of the kinks. Now, in the compacton bearing system, there exist a large number of internal modes which are excited during the collision. Then, the energy-exchange processes occur in one part between the internal modes, and in the other part between the internal modes and the c.m. mode. In this situation, the reflection back of two colliding compactons would require that most of the internal modes transfer synchronously their energies to the translation mode. It is clear that this requirement is unlikely to occur in a system which possesses a large number of internal modes with quite different frequencies: hence an unstable bound state after the collision. On the other hand, it is worth reemphasizing that compactons can transform into kinks in the presence of strong noise, thus recovering the ability to execute a collision with reflection, as Fig. 6(d1) shows. This

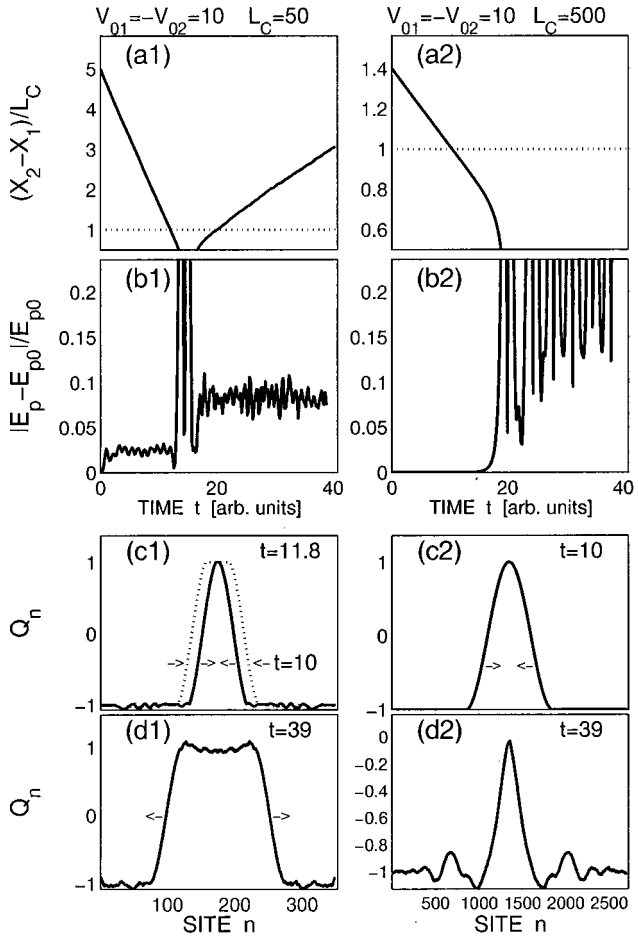

FIG. 6. Plot showing the collision process of a compacton traveling at velocity $V_{01}=10$ and an anticompacton traveling at velocity $V_{02}=-V_{01}$. Time evolution of the normalized separation distance between the center-of-masses of the two compactons for (a1) $L_C=50$ and (a2) $L_C=500$. Time evolution of the interaction energy for (b1) $L_C=50$ and (b2) $L_C=500$. System profile at time (c1) $t=10$ (dotted curve) and $t=11.8$ (solid curve) for $L_C=50$ and (b2) at times $t=10$ for $L_C=500$. (d1) System profile at time $t=39$ for (c1) $L_C=50$ and (d2) $L_C=500$.

conversion of a part of the compacton's energy into noise induces a small drop in the compacton's velocity. Figure 6(c2) shows that in the absence of noise, the *big* compactons ($L_C=500$) come into contact at time $t=10$, at which the small compactons ($L_C=50$) are still clearly separated by approximately $D_{\text{eff}}=27$ lattice sites [as the dotted curve shows in Fig. 6(c1)]. The *small* compactons finally come into contact after few while after the *big* compactons, at time $t=11.8$ [see the solid curve in Fig. 6(c1)].

V. CONCLUSION

In conclusion, we have demonstrated that the ballistic propagation of a CK in nonlinear Klein-Gordon systems is subject to three main limiting factors which may alter its fundamental properties. In the regions of small nonlinear coupling, discreteness effects give rise to a PN potential which provides pinning sites for a CK. On the other hand, a linear coupling gives rise to a phonon band which enters in direct resonance with the internal modes of the CK, causing radiation of energy away from the CK. These two limiting factors are strongly reduced for $C_l \simeq 0$, $C_{\text{nl}} \gg 1$. The existence of a Goldstone mode in this parameter region makes possible a stable ballistic propagation for a CK. The third limiting factor is related to the interactions between compactons: we have shown that in contrast to the pulse compactons introduced by Rosenau and Hyman [5,9] which survive collisions, our CK's do not survive a head-on collision which ends in an unstable bound state. Despite those limiting factors, the ability of a CK to execute a stable ballistic propagation constitutes a potential advantage as regards applications to signal processing. Without being too speculative we suggest that the use of CK's for data transmission purposes would offer as main advantage, compared with usual kink structures [18], the absence of long range interactions between adjacent compactons. This property might be exploited to increase the capacity of fiber links. In view of these remarkable features we believe that the efforts required to generate structures with a compact support in real physical systems deserve to be carried on.

ACKNOWLEDGMENTS

Financial support from the Center National de la Recherche Scientifique, the Ministère de la Recherche et de la Technologie, and the Conseil Régional de Bourgogne is gratefully acknowledged.

[1] M. Peyrard and M. Kruskal, Physica D **14**, 88 (1984).
[2] R. Boesch, C. R. Willis, and M. El-Batanouny, Phys. Rev. B **40**, 2284 (1989).
[3] P. Tchofo Dinda and C. R. Willis, Phys. Rev. E **51**, 4958 (1995).
[4] J. Andrew Combs and Sidney Yip, Phys. Rev. B **28**, 6873 (1983).
[5] P. Rosenau and J. M. Hyman, Phys. Rev. Lett. **70**, 564 (1993).
[6] Yuri S. Kivshar, Phys. Rev. E **48**, 43 (1993).
[7] S. Dusuel, P. Michaux, and M. Remoissenet, Phys. Rev. E **57**, 2320 (1998).
[8] V. V. Konotop and S. Takeno, Phys. Rev. E **60**, 1001 (1999).
[9] P. Rosenau, Phys. Rev. Lett. **13**, 1737 (1994).
[10] J. A. Krumshanl and J. R. Schrieffer, Phys. Rev. B **11**, 3535 (1975).
[11] P. Tchofo Dinda, Phys. Rev. B **46**, 12 012 (1992).
[12] R. Boesch, P. Stancioff, and C. R. Willis, Phys. Rev. B **38**, 6713 (1988).
[13] D. K. Campbell, J. F. Schonfeld, and C. A. Wingate, Physica D **9**, 1 (1983).
[14] M. Peyrard and D. K. Campbell, Physica D **9**, 33 (1983).
[15] D. K. Campbell, M. Peyrard, and P. Sodano, Physica D **19**, 165 (1986).
[16] T. I. Belova and A. E. Kudryavtsev, Physica D **32**, 18 (1988).
[17] F. Zhang, Phys. Rev. E **54**, 4325 (1996).
[18] S. Pitois, G. Millot, and S. Wabnitz, Phys. Rev. Lett. **81**, 1409 (1998).